Static and dynamic nonlinear behavior of a multistable structural system

Carlos H. L. de Castro[1], Rafael J. Pantaleão[1], Diego Orlando[2], Paulo B. Gonçalves[1]

[1]*Dept. of Civil and Environmental Engineering, Pontifical Catholic University of Rio de Janeiro – PUC-Rio*
Rua Marquês de São Vicente, 225, Gávea, 22451-900, Rio de Janeiro/RJ, Brazil
carlos.lima.castro@gmail.com, rafaelpantaleao1@gmail.com, paulo@puc-rio.br
[2]*Dept. of Mechanics and Energy – FAT, State University of Rio de Janeiro – UERJ*
Rodovia Presidente Dutra, km 298, 27537-000, Resende/RJ, Brazil
dgorlando@gmail.com

Abstract. The persistent search for new structural solutions has generated great interest from the scientific community in understanding the static instability and nonlinear dynamics of multistable structural systems. Structural multistability is achieved through structural arrangements that have several stable equilibrium configurations and have a wide field of applications, such as: vibration control, self-deployable and collapsible structures, dynamical systems with a periodic pattern and in the development of new materials (metamaterials), among others. In this work we study the static and dynamic nonlinear behavior of a multistable structural system formed by a sequence of von Mises trusses. For this, the non-linear equilibrium equations and equations of motion, in their dimensionless forms, are obtained through the criterion of minimum potential energy and Hamilton's principle. Based on dimensionless parameters, equipotential energy surfaces and curves, non-linear equilibrium paths, time responses, phase portraits and basins of attraction are obtained. Then a parametric analysis is conducted to identify the influence of the dimensionless parameters on the quantity and stability of equilibrium positions. From the results, the importance of geometric nonlinearity in the dynamics and stability in this new class of structural systems is verified.

Keywords: multistability, nonlinear vibrations, von Mises trusses.

1 Introduction

Structural engineers search for more efficient structural solutions to increasingly different engineering problems. Several recent applications have focused on systems displaying more than one stable equilibrium positions and several studies have been dedicated to the understanding of the static instability and nonlinear dynamics of these multistable structural systems [1-3]. To prevent the loss of stability of the pre-buckling configuration has been for many decades the aim of structural design. However, a new research field in engineering has focused on structures, such as deployable structures [4], that can undergo large displacements and rotations without damage displaying different stable equilibrium positions, with applications beyond civil engineering, for example, within aerospace [5], mechanical [6] and bioengineering [7], or even, in the development of new materials (metamaterials) [8] and dynamical systems with a periodic pattern [9].

Systems with multiple stable configurations can be obtained from the most diverse structural arrangements [10]. Among the multistable mechanisms, the bistable structures can be highlighted, whose best-known example is the basic von Mises truss [11]. In addition to being simple, it can function as an isolated mechanisms or constitute the substructure of more complex structural systems. In this work, the static instability and the nonlinear free vibration of a multistable system formed by a sequence of von Mises trusses is studied. This nonlinear model can be suitably used in the protection of structures, vibration control, construction of self-deployable and collapsible structures or systems that assume many stable configurations throughout their useful life.

2 Problem formulation

The analyzed structural system consists of a sequence of two von Mises trusses linked by rigid bars in such a way that leads to a model with multiple equilibrium configurations, as illustrated in Fig. 1, where a represents the height of the upper truss, b the height of the lower truss, c half length of the truss base, k_1 the axial stiffness of upper truss, k_2 the axial stiffness of lower truss, v_1 the displacement of the upper truss central joint, v_2 the displacement of the lower truss central joint and P the static load applied at the top node.

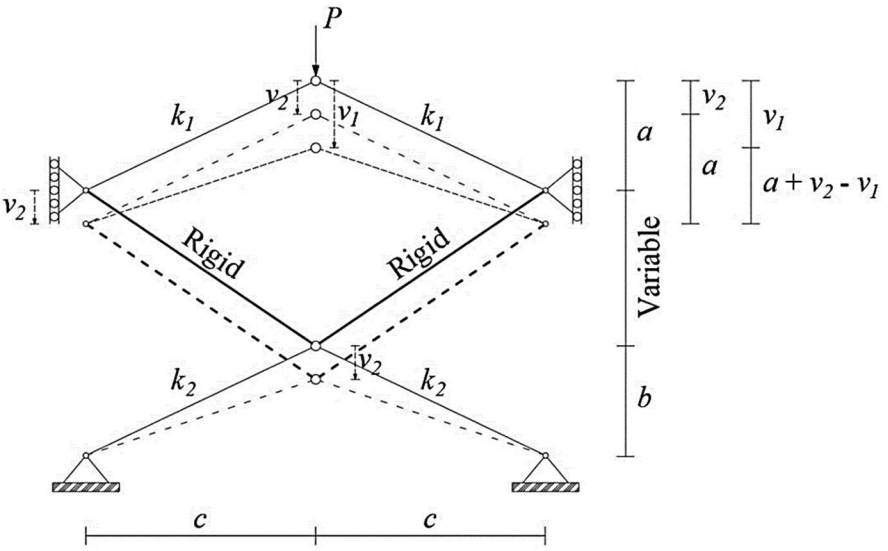

Figure 1. Model with two von Mises trusses coupled

In the undeformed configuration and after application of the load P, the length of each truss bar is given respectively by:

$$L1_i = \sqrt{a^2 + c^2},\ L2_i = \sqrt{b^2 + c^2} \ \text{ and } \ L1_f = \sqrt{\left(a + v_2 - v_1\right)^2 + c^2},\ L2_f = \sqrt{\left(b - v_2\right)^2 + c^2}. \tag{1}$$

Considering the engineering strain (ε), and a linear, elastic material, the strain energy is given by:

$$U_i = \int_0^{Li} \frac{1}{2} k_i \left(\varepsilon_i\right)^2 dx, \ \text{ where } \ \varepsilon_i = \frac{\Delta Li}{Li} = \frac{Li_f - Li_i}{Li_i}. \tag{2}$$

Taking the contribution of each truss bar, the internal strain energy (U) and the gravitational potential energy of the applied load (V) are given by:

$$U = k_1 L1_i \left(\frac{L1_f - L1_i}{L1_i}\right)^2 + k_2 L2_i \left(\frac{L2_f - L2_i}{L2_i}\right)^2 \ \text{ and } \ V = -P v_1. \tag{3}$$

So, the total potential energy of the system ($\Pi = U + V$) is:

$$\Pi = k_1 L1_i \left(\frac{L1_f - L1_i}{L1_i}\right)^2 + k_2 L2_i \left(\frac{L2_f - L2_i}{L2_i}\right)^2 - P v_1. \tag{4}$$

The kinetic energy is given by:

$$T = \frac{\rho A_0 \sqrt{a^2 + c^2}}{3} \dot{v}_1^{\,2} + \left(\rho A_0 \sqrt{a^2 + c^2} + \frac{\rho A_0 \sqrt{b^2 + c^2}}{3}\right) \dot{v}_2^{\,2}. \tag{5}$$

where the overdot represent the displacement derivative with respect to time, ρ is material density and A_0 the undeformed cross section of the bar.

To facilitate the parametric analysis, the following dimensionless parameters are adopted:

$$a=\delta_1 c,\ b=\delta_2 c,\ k_2=\alpha k_1,\ P=\lambda k_1,\ v_1=\chi_1 a, v_2=\chi_2 a,\ \tau=\omega_0 t,\ \omega_0^{\,2}=\frac{k_1}{\rho A_0 c^2},\ \bar{\Pi}=\frac{\Pi}{k_1 c}\ \text{and}\ \bar{T}=\frac{T}{k_1 c}. \tag{6}$$

Then, the total potential energy and the kinetic energy can be rewritten in a dimensionless form as:

$$\bar{\Pi}=\sqrt{\delta_1^{\,2}+1}\left(\frac{\sqrt{\left(-\delta_1\chi_1+\delta_2\chi_2+\delta_1\right)^2+1}}{\sqrt{\delta_1^{\,2}+1}}-1\right)^2+\alpha\sqrt{\delta_2^{\,2}+1}\left(\frac{\sqrt{\left(-\delta_2\chi_2+\delta_2\right)^2+1}}{\sqrt{\delta_2^{\,2}+1}}-1\right)^2-\lambda\chi_1\delta_1. \tag{7}$$

$$\bar{T}=\frac{\delta_1^{\,2}\sqrt{\delta_1^{\,2}+1}}{3}\chi_{1,\tau}{}^2+\delta_1^{\,2}\left(\sqrt{\delta_1^{\,2}+1}+\frac{\sqrt{\delta_2^{\,2}+1}}{3}\right)\chi_{2,\tau}{}^2. \tag{8}$$

Now, using the Langrage function ($\bar{L}=\bar{T}-\bar{\Pi}$) and the Hamilton's principle, the two nondimensional equations of motion takes the form:

$$\frac{2\delta_1\sqrt{\delta_1^{\,2}+1}}{3}\chi_{1,\tau\tau}+2\xi_1\delta_1\chi_{1,\tau}+\frac{2\left(\sqrt{\left(\delta_1+\chi_2\delta_2-\chi_1\delta_1\right)^2+1}-\sqrt{\delta_1^{\,2}+1}\right)\left(-\delta_1-\chi_2\delta_2+\chi_1\delta_1\right)}{\sqrt{\delta_1^{\,2}+1}\sqrt{\left(\delta_1+\chi_2\delta_2-\chi_1\delta_1\right)^2+1}}-\lambda=\bar{Q}. \tag{9}$$

$$\begin{aligned}2\delta_2\left(\sqrt{\delta_1^{\,2}+1}+\frac{\sqrt{\delta_2^{\,2}+1}}{3}\right)\chi_{2,\tau\tau}+2\xi_2\delta_2\chi_{2,\tau}+\frac{2\left(\sqrt{\left(\delta_1+\chi_2\delta_2-\chi_1\delta_1\right)^2+1}-\sqrt{\delta_1^{\,2}+1}\right)\left(\delta_1+\chi_2\delta_2-\chi_1\delta_1\right)}{\sqrt{\delta_1^{\,2}+1}\sqrt{\left(\delta_1+\chi_2\delta_2-\chi_1\delta_1\right)^2+1}}\\+\frac{2\alpha\left(\sqrt{\left(\delta_2-\chi_2\delta_2\right)^2+1}-\sqrt{\delta_2^{\,2}+1}\right)\left(-\delta_2+\chi_2\delta_2\right)}{\sqrt{\delta_2^{\,2}+1}\sqrt{\left(\delta_2-\chi_2\delta_2\right)^2+1}}=\bar{Q}.\end{aligned} \tag{10}$$

where $\bar{Q}=Q/k_1$ and ξ_1 and ξ_2 are the damping ratios.

3 Static analysis

3.1 Stability analysis

The behavior of the structure can be described by the nonlinear equilibrium equations, obtained through the minimum potential energy criterion:

$$d\bar{\Pi}/d\chi_i=0,\quad i=1,2. \tag{11}$$

The nonlinear equilibrium paths considering the dimensionless parameters α = 1.0 and $\delta_1=\delta_2$ = 0.1, Fig. 2, shows the typical behavior of a shallow system with six limit points (bifurcations). The critical load is λ_{cr} = 3.81 × 10^{-4}. The solid lines represent stable equilibrium states and dashed lines the unstable equilibrium states. At two limit points of the primary path an unstable symmetric bifurcation occurs simultaneously, giving rise to two additional paths, each with two limit points.

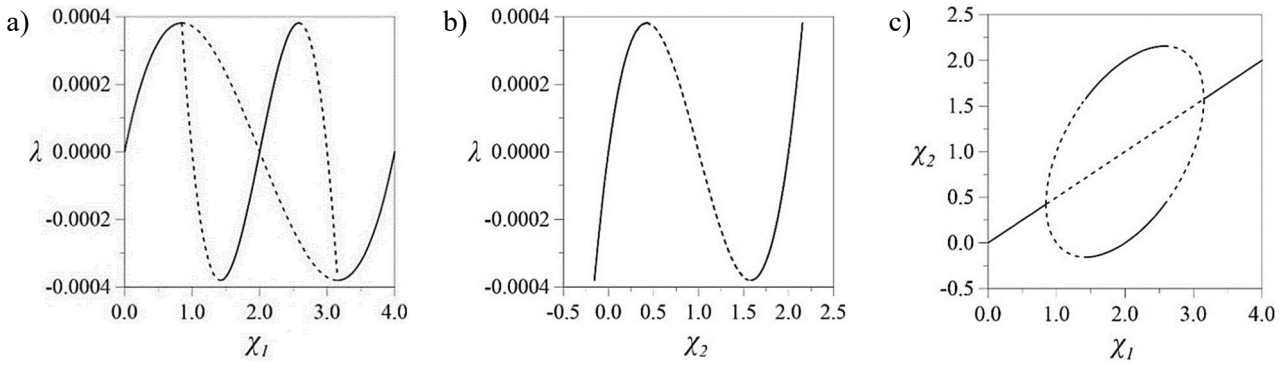

Figure 2. Nonlinear equilibrium path: a) $\lambda \times \chi_1$, b) $\lambda \times \chi_2$ and c) $\chi_1 \times \chi_2$

3.2 Variation of the potential energy

The total potential energy surfaces for $\alpha = 1.0$, $\delta_1 = \delta_2 = 0.1$ and increasing static load levels are shown in Fig. 3. The multistable characteristic of the structural system is evident from the presence of the four potential wells. The unstable configurations are either saddles or maxima.

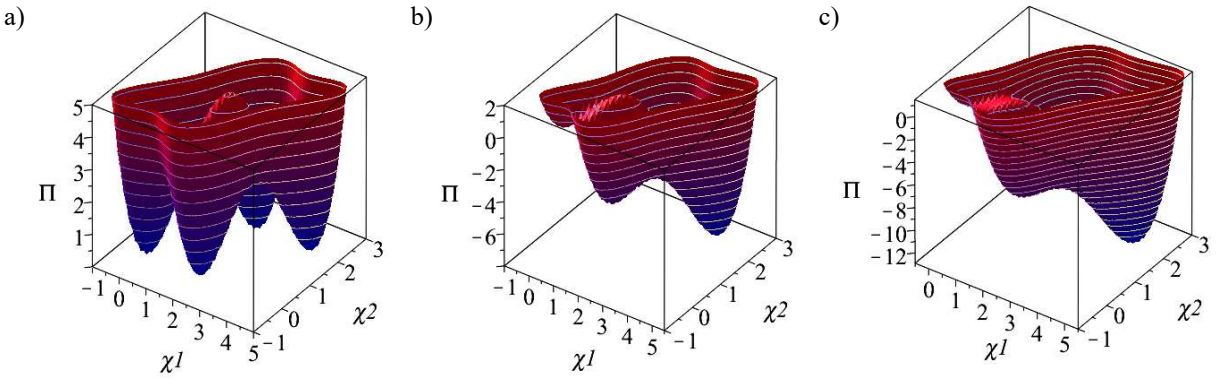

Figure 3. Potential energy variation (surface) with static load level: a) $\lambda = 0.0$ b) $\lambda = 1.8 \times 10^{-4}$ c) $\lambda = 3.15 \times 10^{-4}$

In order to better visualize the equilibria, Fig. 4 presents the equipotential energy curves for increasing static load levels. The dots represent the maximum in red, the minima in blue and saddles in black. For $\lambda = 0.0$, Fig. 4a), four equilibrium configurations of the structural system are observed: one pre-critical, (0,0), and three pos-critical ((2,0), (2,2) and (4,2)). There is also the presence of the five unstable configurations: one maximum point, (2,1), and four saddles (1.0), (1,1), (3.1) and (3.2). Figures 4b) and c) show the influence of the static load on the potential energy, decreasing the safe region associated with the pre-buckling equilibrium configuration.

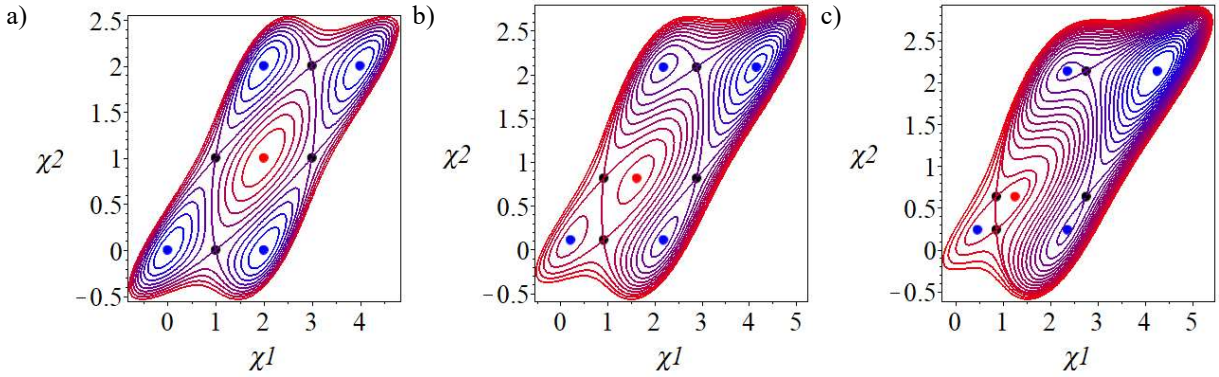

Figure 4. Variation of the curves of equipotential energy with the static load level: a) $\lambda = 0.0$ b) $\lambda = 1.8 \times 10^{-4}$ c) $\lambda = 3.15 \times 10^{-4}$

4 Dynamic free vibration analysis

4.1 Natural frequentes

Expanding the equations of motion, eq. (9) and (10), in Taylor series, retaining the linear terms and considering $\xi_1 = \xi_2 = 0$ and $P = 0$, the following eigenvalue problem is obtained:

$$\left[[K]-\gamma[M]\right] X = 0 \text{ where } \gamma = \bar{\omega}^2 \text{ and } X = \{\chi_1 \quad \chi_2\}^T. \tag{12}$$

where K is the dimensionless stiffness matrix, M the dimensionless mass matrix and $\bar{\omega}$ is the natural frequency parameter.

Solving the eigenvalue problem, the natural frequencies and vibration modes are obtained. Table 1 illustrate de results for selected values of the dimensionless parameters. Analyzing the results, the fundamental mode associated with the lowest frequency corresponds to both trusses moving in the same direction with the same intensity, while the second mode leads to displacements in opposite directions, with $\chi_1 > \chi_2$.

Table 1. Frequencies and associated modes

α	δ_1	δ_2	First ω_0	Eigenvector	Second ω_0	Eigenvector
1.0	0.050	0.050	0.037752317	[1.0 1.0]	0.098836849	[−3.236067987 1.236067978]
1.0	0.100	0.100	0.074943956	[1.0 1.0]	0.196205825	[−3.236067975 1.236067978]
1.0	0.050	0.051	0.038465926	[1.0 1.0]	0.098942698	[−3.271094238 1.272250849]
1.0	0.051	0.050	0.037787191	[1.0 1.0]	0.100700887	[−3.200182188 1.201377445]
0.9	0.050	0.050	0.035908370	[1.0 1.0]	0.098579832	[−3.308871405 1.208871400]
1.1	0.050	0.050	0.039489178	[1.0 1.0]	0.099101620	[−3.164158992 1.264158982]

To study the variation of fundamental frequency with the static load, it is necessary to consider that the total displacement (χ_{nT}) corresponds to the sum of static ($\chi_n i$) and dynamic ($\chi_n(t)$) displacements, that is:

$$\chi_{nT} = \chi_n(t) + \chi_n i. \tag{13}$$

From this change of variables and considering the displacements associated with the pre-buckling positions for increasing levels of static load, according to nonlinear equilibrium path (Fig. 2), the fundamental frequency is obtained. Figure 5 shows the nonlinear frequency-load relation, where the lowest frequency becomes zero at the bifurcation point.

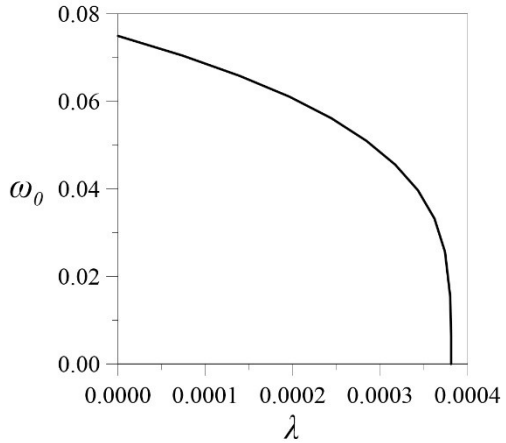

Figure 5. Variation of the natural frequency with the static load level along the pre-buckling path for $\alpha = 1.0$ and $\delta_1 = \delta_2 = 0.1$

4.2 Free vibration response

Considering a conservative system, from eq. (7) and (8), the conservation of energy principle leads to:

$$\overline{\Pi} + \overline{T} = C \tag{14}$$

where C is a given constant associated with the energy level for a set of initial conditions and a given static load level.

Choosing a static equilibrium position, a four-dimensional phase space is obtained: χ_1, $\chi_{1,\tau}$, χ_2 and $\chi_{2,\tau}$. Figure 6 illustrates the four cross-sections of the phase portraits for increasing energy levels and confirms the results of the previous analyses, including the existence of four centers and four saddles. The heteroclinic orbits connecting the saddles separate de different types of motion of the system, including in-well and cross-well motions.

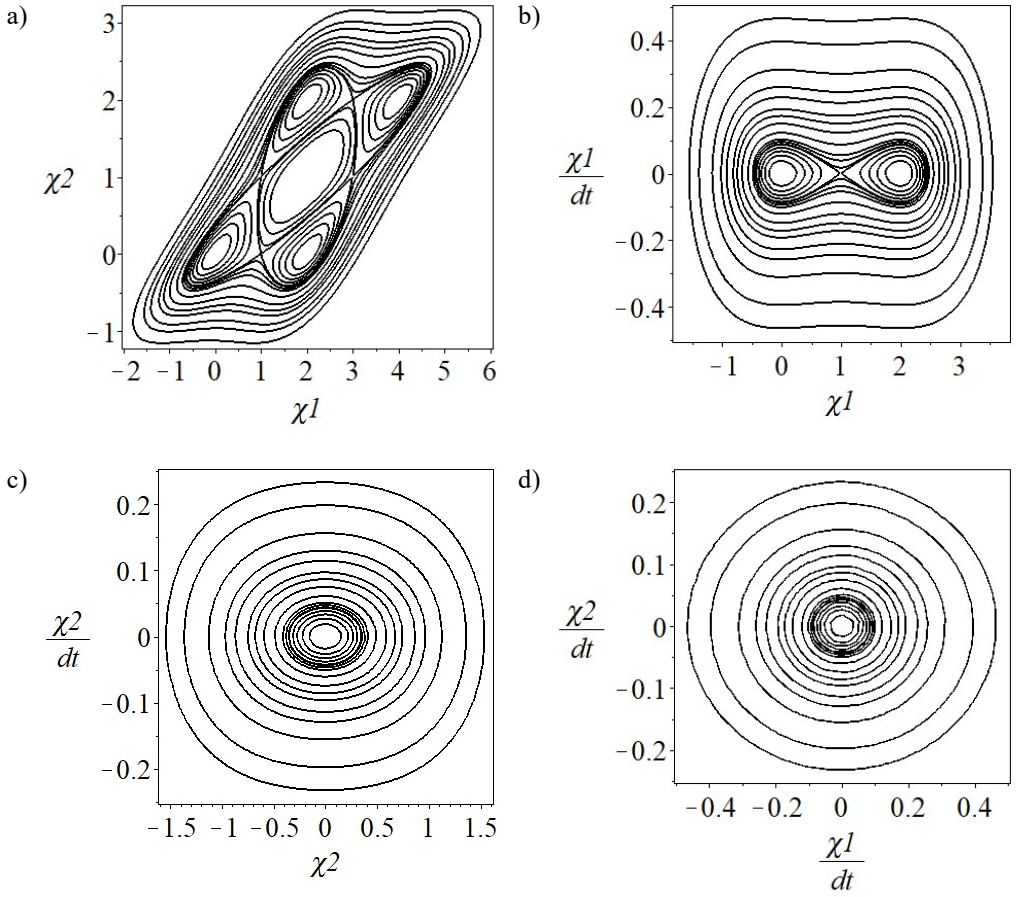

Figure 6. Level energy curves with zero static load ($\lambda = 0.0$) for $\alpha = 1.0$ and $\delta_1 = \delta_2 = 0.1$. a) $\chi_1 \times \chi_2$, b) $\chi_1 \times \chi_{1,\tau}$, c) $\chi_2 \times \chi_{2,\tau}$ and d) $\chi_{1,\tau} \times \chi_{2,\tau}$

However, the dissipative effect of damping must be considered and for each set of initial conditions the damped response will converge to one of the four coexisting attractors. Figure 7 shows the basins of attraction of the damped unloaded system. The yellow points represent the saddles and the white points are the attractors. The blue region denotes the pre-buckling basin of attraction while the black, red and green regions, the basins of attraction of the three pos-buckling configurations. As the static load increases, the basin of attraction associated with pre-buckling equilibrium position decreases, decreasing its dynamic integrity, and most initial conditions are connected to the green basin, the post-buckling equilibrium position where the two trusses are in an inverted position.

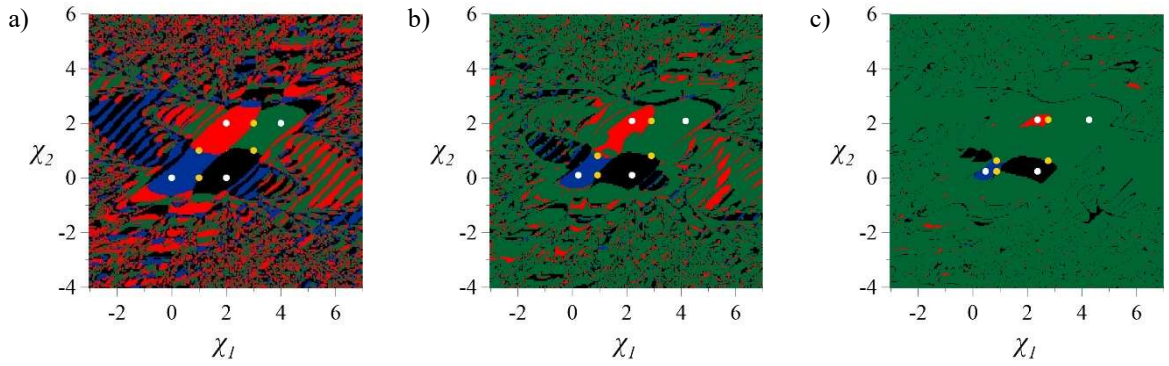

Figure 7. Basins of attraction for $\alpha = 1.0$ and $\delta_1 = \delta_2 = 0.1$. a) $\lambda = 0.0$ b) $\lambda = 1.8 \times 10^{-4}$ c) $\lambda = 3.15 \times 10^{-4}$. The attractor's coordinates are: a) (0.00, 0.00), (2.00, 0.00), (2.00, 2.00), (4.00, 2.00), b) (0.22, 0.11), (2.19, 0.11), (2.19, 2.08), (4.16, 2.08) and c) (0.47, 0.24), (2.37, 0.24), (2.37, 2.13), (4.27, 2.13)

5 Conclusions

This work illustrates the complex static behavior of multistable systems. Due to the geometric nonlinearity and to the fact that each truss exhibit two stable equilibrium positions, the proposed structural system exhibit both limit point and unstable symmetric bifurcations, leading to three equilibrium paths and four coexisting stable solutions. The influence of the static load is demonstrated by the significant changes in the four potential wells, equipotential energy curves and basins of attraction. The evolution of the potential energy and basins of attraction reveal the great sensitivity of the pre-buckling equilibrium configuration to the static load levels. Future work will include the nonlinear dynamic behavior of this model to assess its safety.

Acknowledgements. The authors acknowledge the financial support of the Brazilian research agencies CAPES, CNPq and FAPERJ.

Authorship statement. The authors hereby confirm that they are the sole liable persons responsible for the authorship of this work, and that all material that has been herein included as part of the present paper is either the property (and authorship) of the authors, or has the permission of the owners to be included here.

References

[1] Aza, C.; Pirrera, A.; Schenk, M. Multistable trusses of nonlinear morphing elements. In: *2018 International Conference on Reconfigurable Mechanisms and Robots (ReMAR)*. Delft, Holanda, 2018, p. 1-6.
[2] Benedetti, K. C. B.; Gonçalves, P. B.; Silva, F. M. A. Nonlinear oscillations and bifurcations of a multistable truss and dynamic integrity assessment via a Monte Carlo approach. *Meccanica*, v. 55, p. 2623–2657, 2020.
[3] Falope, F. O.; Pelliciari, M.; Lanzoni, L.; Tarantino, A. M. Snap-through and Eulerian buckling of the bi-stable von Mises truss in nonlinear elasticity: A theoretical, numerical and experimental investigation. *International Journal of Non-Linear Mechanics*. v. 134, p. 103739, 2021.
[4] Santana, M. V.; Arnouts, L. I. W.; Massart, T. J.; Gonçalves, P. B.; Berke, P. Z. Corotational 3D joint finite element tailored for the simulation of bistable deployable structures. *Engineering Structures*, v. 227, p. 111387, 2021.
[5] Cherston, J.; Strohmeier, P.; Paradiso, J. A. Grappler: Array of bistable elements for pinching net-like infrastructure to low gravity bodies. In: *AIAA Scitech 2019 Forum*. San Diego, California, 2019, p. 0871.
[6] Haddab, Y.; Aiche, G.; Hussein, H.; Salem, M. B.; Lutz, P.; Rubbert, L.; Renaud, P. Mechanical bistable structures for microrobotics and mesorobotics from microfabrication to additive manufacturing. In: *2018 International Conference on Manipulation, Automation and Robotics at Small Scales (MARSS)*. Nagoya, Japan, 2018, p. 1-6.
[7] Kidambi, N.; Zheng, Y.; Harne, R. L.; Wang, K. W. Energy release for the actuation and deployment of muscle-inspired asymmetrically multistable chains. In: *SPIE Smart Structures and Materials + Nondestructive Evaluation and Health Monitoring*. Denver, Colorado, USA. 2018, p. 1059510.
[8] Hua, J.; Lei, H.; Gao, C.; Guo, X.; Fang, D. Parameters analysis and optimization of a typical multistable mechanical metamaterial. *Extreme Mechanics Letters*. v. 35, p. 100640, 2020.
[9] Vincent, U. E.; Kenfack, A. Bifurcation and chaos in coupled periodically forced non-identical Duffing oscillators. *Chaotic Dynamics*, Jul. 2006. Available on: <https://arxiv.org/pdf/nlin/0607074.pdf> Access on: 22 may 2021.
[10] Santer, M.; Pellegrino, S. Compliant multistable structural elements. *International Journal of Solids and Structures*, v. 45, n. 24, p. 6190-6204, 2008.
[11] Orlando, D.; Castro, C. H. L. de; Gonçalves, P. B. Nonlinear vibrations and instability of a bistable shallow reticulated truss. *Nonlinear Dynamics*, v. 94, n. 2, p. 1479-1499, 2018.